Deformed Phthalocyanines: Synthesis and Characterization of Zinc Phthalocyanines Bearing Phenyl Substituents at the 1-, 4-, 8-, 11-, 15-, 18-, 22-, and/or 25-Positions

Takamitsu Fukuda, Shigetsugu Homma, and Nagao Kobayashi*[a]

Abstract: The synthesis of a series of zinc phthalocyanines partially phenyl-substituted at the 1-, 4-, 8-, 11-, 15-, 18-, 22-, and/or 25-positions (the so-called α-positions) is reported. Macrocycle formation based on 3,6-diphenylphthalonitrile, *o*-phthalonitrile, and zinc acetate predominantly yielded the near-planar disubstituted complex and opposite tetrasubstituted isomer, while the lithium method yielded the sterically hindered hexasubstituted complex and adjacent tetrasubstituted isomer. All compounds have been characterized by ^{1}H NMR, MALDI-TOF-MS, and elemental analysis methods. In addition, crystal structures have been solved for the di-, hexa-, and octasubstituted complexes and the adjacent tetrasubstituted isomer. DFT geometry optimization calculations predict more highly deformed structures than those observed in the crystals. The packing force of the crystals cannot therefore be ignored, particularly for the less phenyl-substituted derivatives. The crystal structures have revealed that overlap of the phenyl groups causes substantial deformation of the phthalocyanine (Pc) ligands within the crystals, while strong π–π stacking in the remainder of the Pc moiety lacking phenyl substituents can suppress the impact of the deformation. Absorption spectra show sizable red shifts of the Q-band with increasing number of phenyl groups. Analysis of the results of absorption spectra and electrochemical measurements reveals that a substantial portion of the red shift is attributable to the ring deformations. Molecular orbital calculations lend further support to this conclusion. A moderately intense absorption band emerging at around 430 nm for highly deformed octaphenyl-substituted zinc Pc can be assigned to the HOMO→LUMO+3 transition, which is parity-forbidden for planar Pcs, but becomes allowed since the ring deformations remove the center of symmetry.

Keywords: dyes/pigments · electronic structure · phthalocyanines · porphyrinoids · UV/Vis spectroscopy

Introduction

The discovery of phthalocyanine (Pc) dates back to the early 20th century. Braun and Tcherniac first reported a Pc-like substance in 1907.[1] The structure of Pc was subsequently confirmed by X-ray crystallography by Robertson in 1935 and 1936.[2] Since then, Pcs have been developed as industrial dyes and pigments due to their intense colors and high chemical and physical stability. Today, more than fifty thousand tonnes of Pcs are produced annually around the world. In addition, the versatile spectroscopic and electrochemical properties of Pcs have attracted the interest of researchers in a variety of leading-edge fields. A large number of papers and patents have been published.[3] Applications including use in write-read optical discs, nonlinear optics, as catalysts, in deodorants, as electrical conductors, in semiconductors, and in photodynamic cancer therapy have been developed in recent years. Most α- and/or β-position[4]-substituted Pc monomers have been confirmed as having highly planar molecular structures by X-ray crystallography.[5] The most notable exceptions have tended to be metallo-Pcs in which the central metal has a large ionic radius.[6] Reports on nonplanar substituted Pcs have begun to appear only recently. Cook's group reported the crystal structure of a conformationally stressed 1,4,8,11,15,18,22,25-octaisopentyl H_2Pc,[7] while we independently reported a highly deformed α-octaphenylated H_2Pc (H_2PcPh_8).[8] Gorun and co-workers have since characterized the first dome-shaped metal-free Pc in the solid state.[9] Spectroscopic evidence of ligand deformation in solution was found in the case of $FePcPh_8$, where the

[a] Dr. T. Fukuda, S. Homma, Prof. Dr. Dr. N. Kobayashi
Department of Chemistry, Graduate School of Science
Tohoku University, Sendai 980–8578 (Japan)
Fax: (+81) 22-795-7719
E-mail: nagaok@mail.tains.tohoku.ac.jp

Supporting information (^{1}H NMR spectra of **2**, **5**, and **6**. Views of the frontier orbitals of **2**–**5**) for this article is available on the WWW under http://www.chemeurj.org/ or from the authors.

 DOI: 10.1002/chem.200500176

originally parity-forbidden MLCT transitions became allowed as a consequence of ring saddling.[10] Metal $PcPh_8$ complexes also show unusual spectral band shifts, which are sufficiently large to result in red or ochre colors both in the solid phase and in solution.[11] These salient features of the α-phenyl-substituted Pc prompted us to investigate the relationship between the spectroscopic and electrochemical properties and the molecular structures. In this study, we report the synthesis of a series of α-phenyl-substituted ZnPcs **1**–**6** (Figure 1). Compounds **4**, **5**, and **6** are expected

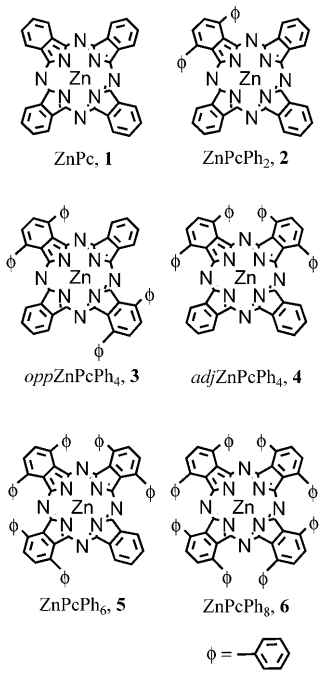

Figure 1. Structures and abbreviations of the compounds used in this study.

to have deformed ligands due to the steric hindrance of adjacent phenyl groups, while conversely compounds **1**, **2**, and **3** are expected to be planar. The substituent effects of α-phenyl groups can be estimated by comparing **1**, **2**, and **3**, while the ring deformation effects are examined using **4**, **5**, and **6**. Many papers concerning deformed aromatic systems, including pyrene,[12] buckminsterfullerene,[13] porphyrin,[14] and subphthalocyanine[15] derivatives, have been published to date. Nonplanar Pcs are of interest in a variety of fields due to the intense red-shifted Q-bands and the potential for novel forms of metal–ligand *d*-π interaction.

Results and Discussion

Synthesis: In general, Pc monomers can incorporate one transition metal ion or two protons within the central cavity.[16] Since the focus of this study was ligand deformation effects, and not ligand–metal interactions, the central metal had to be chosen carefully. Fe^{II} complexes, for example, show significant metal–ligand interactions,[10,17] and are therefore unsuitable. Free base, Si^{IV}, Ni^{II}, or Zn^{II} derivatives were possible candidates, since their NMR measurements for structural characterizations are straightforward, and a large number of papers on their planar complexes have been published.[16] The first three have significant drawbacks in terms of the effective symmetry for spectroscopic studies in the case of metal-free ligands, solubility, and complex synthetic procedures in the case of Si^{IV} complexes. ZnPcs have fairly high solubilities in coordinating solvents such as pyridine, and no significant metal–ligand interactions are expected due to the closed-shell d^{10} configuration.[18] Thus, Zn^{II} was chosen as the central metal. As has already been noted in our recent papers,[19,20] the lithium method often tends to produce adjacent-type isomers (i.e., **4**), even in the presence of protruding α-phenyl substituents, probably via so-called "half-Pc" intermediates.[21] In contrast, template reactions using Zn^{II} ions in the absence of base usually produce the opposite isomers (i.e., **3**), since this reduces the level of steric repulsion.[22,23] We have therefore performed mixed condensations using *o*-phthalonitrile and 3,6-diphenylphthalonitrile, employing both methods. In the case of the lithium method, $ZnPh_2Pc$ (**2**) was obtained in 16.5% yield (based on the total mixed nitrile), along with sterically hindered **4** and **5** in yields of 2.7 and 7.1%, respectively, while little of the opposite isomer, **3**, could be isolated. Taking into account the 2:1 molecular ratio of precursors, a statistical distribution of these derivatives would afford 19.8% of **4** and 9.9% of **5**. Therefore, **4** and **5** were obtained in respective yields of 13.6 and 71.7% with respect to the theoretical distribution. Although **6** was also obtained, this compound was prepared separately to simplify the purification procedures. Conversely, a metal template reaction based on zinc acetate resulted in the formation of **2** and **3** in respective yields of 10.5 and 3.4% (26.6 and 34.3% yields with respect to the theoretical 39.5 and 9.9%). Formation of the sterically hindered derivatives (**4**, **5**, and **6**) was negligible. Differences in the reaction mechanism contribute to the observed differences in the formation ratios. Template reactions using transition metals require the simultaneous assembly of four reactant nitrile molecules,[24] which hinders Pc formation, while the lithium method requires only two nitriles to form half-Pc intermediates.[21]

Structures: All six complexes were first characterized by MALDI-TOF mass spectrometry and elemental analysis. In addition, the structures were confirmed by ^1H NMR spectroscopy and X-ray crystallography (for **2**, **4**, **5**, and **6**). Unfortunately, no crystals of sufficient quality could be obtained for **3**. Figure 2 shows ^1H NMR spectra of the opposite (**3**) and adjacent (**4**) isomers in [D_5]pyridine. From the molecular symmetries, **4** is expected to have a more complex NMR spectrum. As a result, the integrated values for the equivalent protons should be in multiples of four for **3**, and two for **4**. In Figure 2a, the proton environments are grouped into four regions with relative integration values of 4, 8, 8, and 12 from low to high magnetic field. This unambigu-

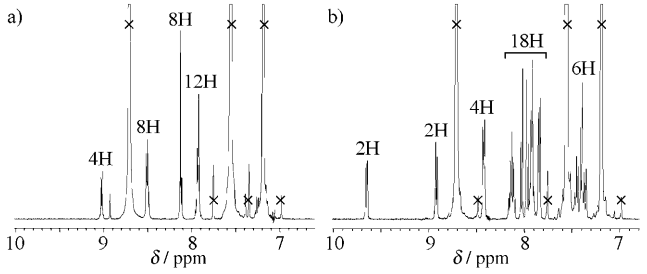

Figure 2. ^{1}H NMR spectra of **3** (a) and **4** (b) in [D_5]pyridine. The × denotes solvent and ^{13}C satellite signals.

ously proves that **3** has an opposite isomer structure. In contrast, Figure 2b features a more complex set of proton signals and the integration values for $\delta = 9.65$ and 8.92 ppm are 2 rather than 4. This confirms that **4** is the adjacent isomer. The ^{1}H NMR spectra of the other complexes (**2**, **5**, and **6**) are supplied in the Supporting Information.

Further evidence for the assignment of the ^{1}H NMR spectra of **3** and **4** was provided by X-ray crystallography. Crystallization took place in pyridine solution during slow evaporation of the solvent, except in the case of **2**, for which a toluene/pyridine 1:1 (v/v) solution was used instead. The crystallographic parameters are summarized in Table 1. Figure 3 and Figure 4 show ORTEP views of **2**, **4**, **5**, and **6**, and the packing arrangements of these complexes and H_2PcPh_8, respectively.[8] Figure 5 and Figure 6 depict colormap analyses[25] of the extent of ring deformation. The displacements of the ligand atoms are calculated relative to the 4N-plane generated by the four pyrrole nitrogens on the inner ligand perimeter. All of the crystals have a pyridine molecule coordinated to the Zn^{II}. Zn^{II} Pcs are normally pentacoordinate.[26] An example of a hexacoordinate crystal has been reported as a special case, however.[27] The pyridine prevents extensive π–π interactions on one side of the Pc and allows close π–π stackings at the opposite side. In the case of **2**, the unit cell contains two discrete Pc ligands (green- and purple-colored regions in Figure 4a) having practically planar conformations. In Figure 5, the colormap is entirely yellowish-green in the case of **2**, indicating a high degree of planarity. Figure 6 confirms this observation. As expected, **5** and **6** have highly deformed structures at neighboring isoindole units where two phenyl groups overlap. In particular, the structure of **6** is similar to that of H_2PcPh_8, where alternating up and down displacements of the isoindole units results in a saddled structure.[8] The maximum deviation of the pyrrole β-carbon atom is about 1.18 Å for **6** (Figure 6), which is comparable to that in H_2PcPh_8, while those of near-planar Pcs are within about 0.15 Å. The deviation is somewhat less for **5**, amounting to 0.76 Å at the site with largest deviation and 0.34 and 0.69 Å at sites adjacent to this. Although the structures of **5** and **6** are in line with what was anticipated, the crystal structure of *adj*$ZnPcPh_4$ (**4**) is not. **4** maintains a relatively high degree of planarity in the crystalline state, Figure 5 and Figure 6, despite the existence of phenyl overlaps. The colormap analysis resembles that of **2**. Figure 6 demonstrates that **4** takes on a ruffled rather than a saddled structure, in which the *meso*-nitrogen atoms lie outside the 4N-plane.[28]

DFT geometry optimizations were conducted for **2**, **4**, **5**, and **6** using the B3LYP functional with 6–31G(d) basis sets, with the results illustrated in the right-hand column of Figure 6. Although the crystal structures and optimized structures of **6** are almost identical, clear differences are observed for **4**. The calculation predicts the anticipated saddled conformations. The origin of the planarity observed in the crystals can be attributed to the packing forces of these complexes. A molecule of **2** stacks with another molecule so that they avoid phenyl overlaps in the crystalline state. As a consequence, **2** adopts a slipped stacked packing structure. The packing structures are basically similar for **5** and **6**. The extent of the stacking displacement changes in the order **4** < **5** < **6**. The overlap area of **4** (Pc-A and Pc-B) is more than 90%, as illustrated in Figure 4, which means that intermolecular interactions are very extensive. On the other hand, the overlap area of **5** decreases to around 25%, and the two Pcs are displaced along the diagonal direction of the Pc. The nonplanarity of **5** observed in the X-ray crystal data (Figure 6) indicates that the phenyl-substituted sites deviate significantly from planarity and that the non-substituted isoindole is near-planar,

Table 1. Crystal data and structure refinement.[a]

Data	**2**	**4**	**5**	**6**
empirical formula	$C_{115}H_{76}N_{20}Zn_2$	$C_{76}H_{52}N_{12}Zn$	$C_{83}H_{50}N_{11}Zn$	$C_{98}H_{63}N_{11}Zn$
formula weight	1868.70	1198.67	1266.71	1459.96
crystal color, habit	dark red, prism	dark red, cubic	dark green, plate	green, plate
crystal dimensions [mm]	0.25×0.20×0.15	0.35×0.35×0.45	0.40×0.20×0.01	0.25×0.15×0.15
crystal system	triclinic	triclinic	triclinic	triclinic
a [Å]	15.155(8)	13.6833(5)	14.599(2)	13.310(3)
b [Å]	16.351(8)	15.5742(7)	15.235(1)	16.255(4)
c [Å]	19.468(9)	16.2391(7)	15.507(2)	16.999(4)
α [°]	94.412(5)	103.7364(9)	72.43(2)	96.207(4)
β [°]	92.372(5)	104.2462(9)	79.72(3)	98.408(4)
γ [°]	112.302(6)	111.3746(9)	65.02(2)	93.006(4)
V [Å^3]	4437(4)	2911.1(2)	2975.4(8)	3608(1)
space group	$P\bar{1}$ (no. 2)	$P\bar{1}$ (no. 2)	$P\bar{1}$ (no. 2)	$P\bar{1}$ (no. 2)
Z	2	2	2	2
ρ_{calcd} [g^{-1}cm^{-3}]	1.399	1.367	1.414	1.344
temperature [K]	223	173	173	173
residuals R/Rw	0.063/0.130	0.044/0.109	0.080/0.197	0.069/0.139
goodness-of-fit indicator	1.12	1.02	1.13	1.08

[a] CCDC 263814–263817 contain the supplementary crystallographic data for this paper. These data can be obtained free of charge from The Cambridge Crystallographic Data Centre via www.ccdc.cam.ac.uk/data_request/cif.

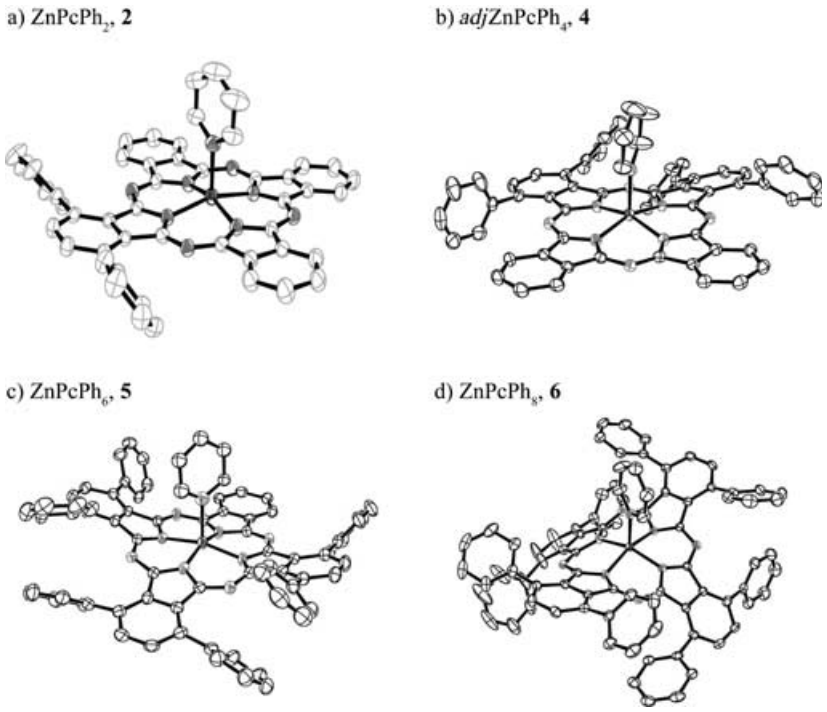

Figure 3. View of the molecular structures of a) **2**, b) **4**, c) **5**, and d) **6**. Displacement ellipsoids are shown at the 50% probability level. Hydrogen atoms have been omitted for clarity.

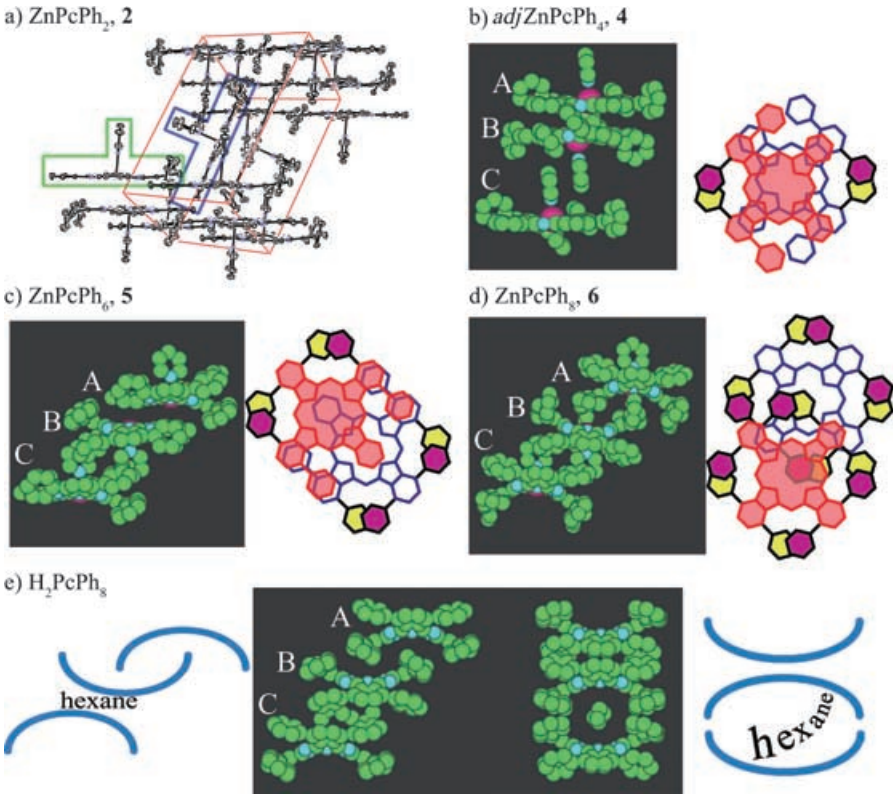

Figure 4. ORTEP (a) and CPK models (b–d) of the packing arrangements of the crystals **2**, **4**, **5**, and **6,** as well as the stacking structures. e) For comparison purposes, the packing arrangement of H_2PcPh_8 is shown.

while the DFT-optimized structure shows that even non-phenyl-substituted isoindoles deviate from planarity to some degree. These observations strongly suggest that the folding of the Pc ligand probably extends to the non-phenyl-substituted isoindoles in solution, but the π–π stacking interactions are sufficient to enforce a local planar structure in the crystalline state.[29] In the case of **6**, however, virtually no stacking is observed between Pc-A and Pc-B, indicating that intermolecular interactions are small. The average dihedral angles defined by the fused benzo rings and the substituted phenyl groups are 57° and 49° at the overlapping sites and the other open sites, respectively. In other words, no significant differences are observed due to steric crowding. It can therefore be concluded that a folded conformation rather than a decreased dihedral angle of the phenyl groups is the mechanism favored energetically to reduce the intramolecular hindrances.[30] Interestingly, the previously reported H_2PcPh_8 was also found to adopt a similar packing arrangement to **6**, despite the fact that H_2PcPh_8 has no axial ligand. As a consequence, the crystals have a nanoscale porous structure between Pc-B and Pc-C with dimensions of approximately $0.74 \times 0.77\ nm^2$ (Figure 4e), which can accommodate one hexane molecule in the void as a guest.

Electronic absorption and MCD spectroscopy: Figure 7 shows the absorption and MCD spectra of **1–6** in pyridine. The wavelength data are tabulated in Table 2. All of the complexes, with the exception of **3**, exhibit an intense, unresolved, Q-band in the 650–850 nm region, which shifts to the red

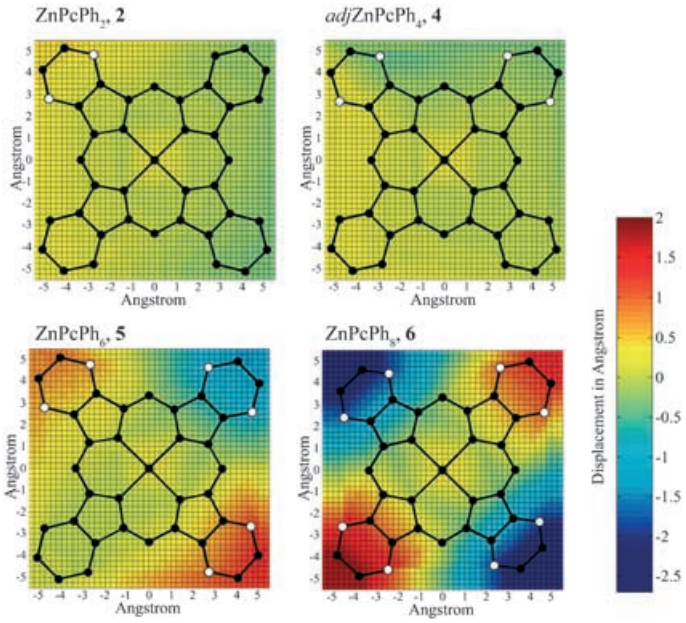

Figure 5. Colormap analyses of the crystal structures of **2**, **4**, **5**, and **6**. Hydrogen atoms and peripheral and axial substituents are omitted for clarity. White marks indicate phenyl-substituted carbon atoms.

as the number of phenyl groups is increased. **1** has a sharp Q-band at 674 nm and the corresponding MCD signal is a typical derivative-shaped Faraday *A*-term, while near-planar phenyl-substituted **2** and **3** show slightly red-shifted Q-bands relative to **1**. The Q-band shifts are summarized in Figure 8a. The Q-band of **3** splits into two components. The splitting is less than 350 cm^{-1}, so the corresponding MCD

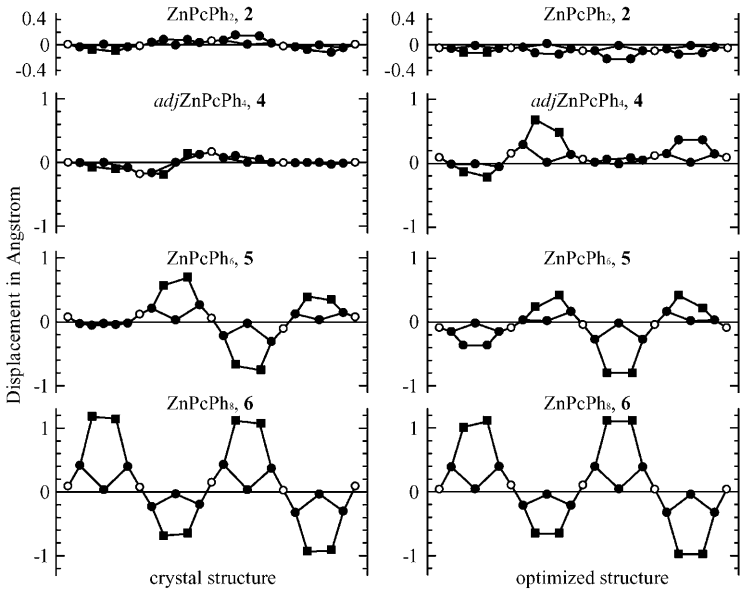

Figure 6. Linear display of the out-of-4 N-plane deviations from planarity for the core atoms of **2**, **4**, **5**, and **6** from top to bottom, respectively. Crystal data are shown in the left-hand column, and optimized geometry data in the right-hand column. The squares indicate carbon atoms bearing phenyl substituents. The *meso*-nitrogen atoms are shown by empty circles.

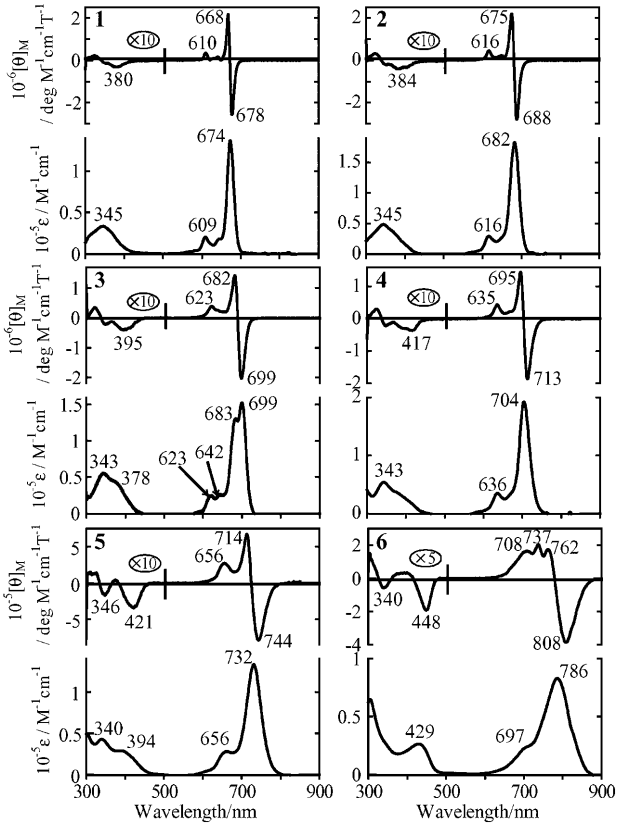

Figure 7. Absorption and MCD spectra of **1**–**6** in pyridine.

signal can be regarded as a pseudo *A*-term. Taking the midpoint of the split Q-band as the Q-band energy of **3**, the Q-band shifts from **1** to **2** and from **2** to **3** are around 170 and 190 cm^{-1}, respectively. The substituent effect of the phenyl groups clearly shifts the Q-band slightly to the red.[31] Partial peripheral substitution usually results in an approximately linear shift of the Q-band energies as the number of substituents is increased.[32,33] It should be noted that although both **3** and **4** contain four phenyl groups, the Q-band of **4** occurs at longer wavelength, by about 270 cm^{-1}. Figure 8a demonstrates that linearity is only valid for the relatively planar **1**–**3**, and that marked deviations from linearity are observed for the deformed complexes **4**–**6**. The shift increases to around 270, 540, and 940 cm^{-1} for **3**→**4**, **4**→**5**, and **5**→**6**. The Q-band shift increases for **4**, **5**, and **6** are therefore primarily due to the increasing ligand folding.

DiMagno[34] and Ghosh[35] and their co-workers have investigated analogous deformation effects for sterically crowded porphyrin compounds in detail. They concluded that the sizable red-shifts of the Q-bands for nonplanar porphyrins are not intrinsically due to ring deformation, but result from changes in bond distances and angles within the porphyrin ligand induced by the addition of substituents. This effect is termed in-plane nuclear reorganization

Table 2. Absorption and MCD data in pyridine.

Compound	Absorption[a]			MCD[b]			
ZnPc, **1**	345 (0.33)	609 (0.20)	674 (1.35)	380 (−0.03)	610 (0.33)	668 (2.15)	678 (−2.55)
$ZnPcPh_2$, **2**	345 (0.48)	616 (0.29)	682 (1.82)	384 (−0.04)	616 (0.49)	675 (2.18)	688 (−2.78)
opp$ZnPcPh_4$, **3**	343 (0.47)	378 (0.42)	623 (0.21)	395 (−0.03)	623 (0.32)	682 (1.19)	699 (−1.71)
	642 (0.22)	683 (1.10)	699 (1.29)				
adj$ZnPcPh_4$, **4**	343 (0.54)	636 (0.35)	704 (1.92)	417 (−0.04)	635 (0.43)	695 (1.43)	713 (−1.85)
$ZnPcPh_6$, **5**	340 (0.43)	394 (0.28)	656 (0.27)	346 (−0.02)	421 (−0.03)	656 (0.27)	714 (0.66)
	732 (1.33)			744 (−0.78)			
$ZnPcPh_8$, **6**	429 (0.26)	697 (0.21)	786 (0.83)	340 (−0.01)	448 (−0.04)	708 (0.16)	737 (0.20)
				762 (0.17)	808 (−0.38)		

[a] λ [nm] ($10^{-5}\varepsilon$ [$dm^3 mol^{-1} cm^{-1}$]). [b] λ [nm] ($10^{-6}[\theta]_M$ [$deg\,dm^3 mol^{-1} cm^{-1} T^{-1}$]).

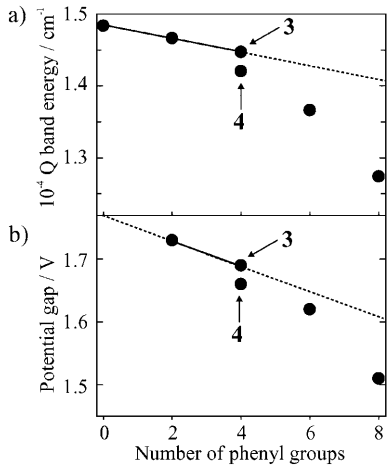

Figure 8. a) Transition of the Q-band energy with respect to the number of phenyl substituents. b) Potential gaps.

(IPNR). On the other hand, Shelnutt and co-workers claimed that higher order B_{1u} deformations of the ligand are the most important factor in producing the observed red shifts, and pointed to the large Soret band shifts seen for highly nonplanar *meso*-tetra(*tert*-butyl) porphyrin relative to *meso*-tetra(methyl)porphyrin, these being primarily the result of nonplanar deformations rather than IPNR.[36] According to these arguments, the noticeable bathochromic shifts of the Q-band for **4**–**6** may stem from either IPNR or B_{1u} ligand deformations. Detailed calculations would be required to ascertain which factor is the more important. Herein, we simply ascribe the observed red-shifts to the effects of ligand deformations. Nonplanarity and IPNR effects are experimentally indistinguishable. When we use the term "ring deformation effects" it implies, therefore, effects caused by both nonplanarity and IPNR. The Q-band broadens with increasing number of phenyl groups, probably because: 1) the low symmetry Pc ligand causes undetectable Q-band splitting, which contributes to the Q-band broadenings; 2) for nonplanar Pcs, dihedral angles between the fused benzo rings and the phenyl groups are not rigidly fixed; for example, the dihedral angles are not identical for the eight phenyl groups in the crystal structure of **6**, which suggests that the deformed Pcs have more conformational flexibility than planar complexes in solution at room temperature. Q-band broadening is therefore considered to be at least partially caused by these structural variations, since the degree of ligand folding determines the Q-band energy.

In the Soret band region (ca. 300–450 nm) of **1**–**3**, one broad band is observed at around 345 nm, accompanied by a less intense, somewhat complex set of MCD signals. In addition, a characteristic band appears at around 400 nm for nonplanar Pcs (i.e., **4**–**6**), with the band at 429 nm for **6** being especially prominent. The origin of these bands is ascribed to the HOMO→LUMO+3 transition, which is parity-forbidden for planar D_{4h} complexes but becomes allowed when ring deformation removes the center of symmetry.[10,37] Details of the band assignments will be discussed with reference to the results of molecular orbital (MO) calculations in the relevant section below.

Electrochemistry: It is well established that the HOMO and LUMO energies of Pc derivatives correlate well with their first oxidation and reduction potentials.[20,22,38] The measurement of electrochemical data is important, therefore, in determining the origins of the red-shifts of the Q-band wavelength. Figure 9 displays cyclic voltammograms of **2**–**6** in *o*-

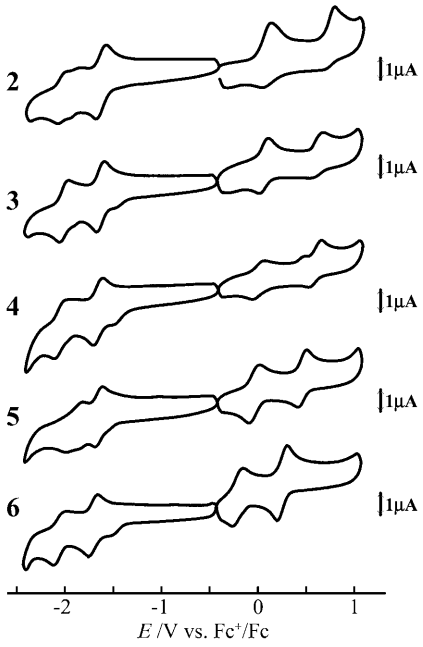

Figure 9. Cyclic voltammograms of **2**–**6** in *o*-DCB containing 0.1 mol L^{-1} TBAP.

DCB with 0.1 mol L^{-1} TBAP as the supporting electrolyte. The redox potential data are tabulated in Table 3 and plotted in Figure 10. Compound **1** is too insoluble in *o*-DCB for satisfactory voltammograms to be obtained.[39,40] Two oxidation and reduction couples were observed for all of the other compounds, with **5** and **6** giving significantly more distinct redox curves in the oxidation region compared to near-planar **2**–**4**, since aggregation is probably accelerated upon oxidation for the less substituted Pcs.[41] From the differences between the various redox potentials (Table 3), all processes are clearly one-electron and can be assigned to either ring oxidation or ring reduction, since Zn^{II} does not undergo redox processes within this potential window.[42,43] In the case of fused-ring expanded Pcs, including naphthalocyanines and anthracocyanines, the HOMO energies increase with decreasing Q-band energies, while the LUMO energies remain relatively stable.[44] A similar trend is observed for compounds **2**–**6**, where the first oxidation potential shifts negatively, while, in contrast, the first reduction potential does not shift appreciably from complex to complex. The first oxidation potentials are +0.10 and −0.20 V (versus Fc^+/Fc) for **2** and **6**, respectively, indicating destabilization of the HOMO by 0.30 V. The first reduction potentials shift to the negative by only 0.08 V on going from **2** to **6**. As a consequence, the energy gap between the first oxidation and reduction potentials decreases from 1.73 to 1.51 V on going from **2** to **6**, as would be anticipated given the observed red-shift of the Q-band. On going from **2** to **3**, the first oxidation potential shifts by 0.04 V, while the first reduction potential remains almost identical (−1.63 V versus Fc^+/Fc), which indicates that the phenyl groups also cause a slight destabilization of the HOMO levels, although the ring deformation effects are much more significant. As shown in Figure 9 and Figure 10, the second oxidation potentials also shift to the negative on going from **2** to **6**, but the second reduction potentials do not shift from ligand to ligand. The relationship between the number of phenyl substituents and the Q-band energies and potential gaps between the first oxidation and reduction couples is shown in Figure 8. Clearly, there is a close relationship between the Q-band energy and potential gap, since both values decrease as the number of phenyl groups is increased. Linearity is maintained only for the planar derivatives, however, with the nonplanar complexes showing significant deviations from the trend. The potential gap of **4** is smaller than that of **3**, as was observed in the analogous Q-band energy values. Thus, the electrochemical results confirm that molecular deformation causes significant destabilization of the HOMO energies, a consequence of which is the bathochromic shifts of the Q-band.

Table 3. Redox potential data (versus Fc^+/Fc) for **2**–**6** in *o*-DCB containing 0.1 M TBAP.[a]

Couple	$E_{1/2}$ [V]	ΔE_p [mV]
$ZnPcPh_2$, **2**		
Pc(+4)/Pc(+3)	+0.76	100
Pc(+3)/Pc(+2)	+0.10	80
Pc(+2)/Pc(+1)	−1.63	100
Pc(+1)/Pc(0)	−1.96	–
opp$ZnPcPh_4$, **3**		
Pc(+4)/Pc(+3)	+0.64	110
Pc(+3)/Pc(+2)	+0.06	100
Pc(+2)/Pc(+1)	−1.63	80
Pc(+1)/Pc(0)	−2.01	100
adj$ZnPcPh_4$, **4**		
Pc(+4)/Pc(+3)	+0.62	100
Pc(+3)/Pc(+2)	+0.01	100
Pc(+2)/Pc(+1)	−1.65	105
Pc(+1)/Pc(0)	−2.06	110
$ZnPcPh_6$, **5**		
Pc(+4)/Pc(+3)	+0.47	80
Pc(+3)/Pc(+2)	−0.03	100
Pc(+2)/Pc(+1)	−1.65	80
Pc(+1)/Pc(0)	−1.92	–
$ZnPcPh_8$, **6**		
Pc(+4)/Pc(+3)	+0.27	90
Pc(+3)/Pc(+2)	−0.20	105
Pc(+2)/Pc(+1)	−1.71	100
Pc(+1)/Pc(0)	−2.07	100

[a] ΔE_p [mV] indicates the potential differences between cathodic and anodic peak potentials at a sweep rate of 50 mV s^{-1}.

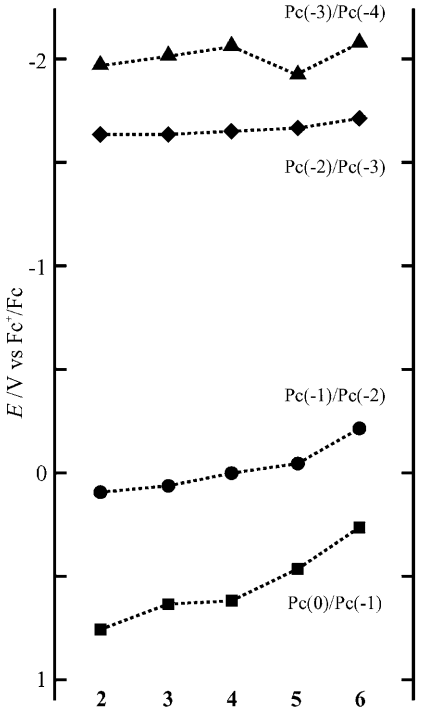

Figure 10. Electrochemically obtained redox data of **2**–**6** in *o*-DCB.

Molecular orbital calculations: Table 4 summarizes the results of the MO calculations. The molecular geometries including a pyridine molecule axially coordinated to the Zn^{II} ion were first optimized at the DFT level using the B3LYP/6–31G(d) combinations of the hybrid functional and basis set as implemented in Gaussian 98.[45] The molecular orbital and excitation energies were calculated using the ZINDO/S method. The transition energies, oscillator strengths, configurations, dipole moments, and polarizations (direction of the transition dipole moments) are listed in the first five col-

Table 4. Calculated transition energies, oscillator strengths (*f*), and configurations.

E [eV]	λ [nm]	*f*	Configuration			Dipole moment	Polarization *x*	*y*	*z*	Phenyl-removed Pc λ [nm]	*f*
ZnPc, **1**											
1.71	724	0.78	108(H)→109(L) (88%)	107→110 (9%)		8.05	1.0	0.0	0.0		
1.72	719	0.80	108→110 (88%)	107→109 (9%)		7.99	0.0	1.0	0.0		
2.16	575	0.00	108→111 (99%)			11.2					
2.80	442	0.00	108→112 (99%)			11.4	0.0	0.0	1.0		
2.89	428	0.00	108→113 (95%)			7.75					
$ZnPcPh_2$, **2**											
1.70	729	0.87	136(H)→137(L) (89%)	134→138 (9%)		7.81	1.0	0.0	0.0	723	0.77
1.72	720	0.78	136→138 (88%)	134→137 (9%)		7.82	0.0	1.0	0.0	718	0.81
2.15	576	0.00	136→139 (99%)			11.2				575	0.00
2.80	443	0.00	136→140 (98%)	136→141 (2%)		11.0	0.4	0.0	0.9	443	0.00
2.87	432	0.00	136→140 (2%)	136→141 (93%)		6.92	1.0	0.0	0.2	428	0.00
opp$ZnPcPh_4$, **3**											
1.68	736	0.95	164(H)→165(L) (89%)	161→166 (8%)		7.56	1.0	0.0	0.0	723	0.77
1.75	710	0.79	164→166 (89%)	161→165 (9%)		7.46	0.0	1.0	0.0	720	0.80
2.15	578	0.01	164→167 (99%)			11.0	0.7	0.7	0.0	578	0.01
2.79	444	0.00	164→168 (100%)			11.9	0.0	0.0	1.0	444	0.00
2.85	435	0.00	164→169 (96%)			7.59	0.0	0.0	1.0	428	0.00
adj$ZnPcPh_4$, **4**											
1.69	733	0.84	164(H)→165(L) (87%)	164→166 (2%)	161→166 (8%)	8.08	0.9	0.4	0.0	730	0.77
1.70	728	0.87	164→165 (2%)	164→166 (87%)	161→165 (8%)	7.57	0.4	0.9	0.1	724	0.79
2.10	590	0.00	164→167 (99%)			11.3	0.0	1.0	0.1	584	0.00
2.74	452	0.00	164→168 (99%)			11.6	0.2	0.2	1.0	448	0.00
2.82	440	0.02	164→169 (47%)	164→170 (42%)	164→171 (6%)	7.66	0.0	0.0	1.0	433	0.01
$ZnPcPh_6$, **5**											
1.66	747	0.84	192(H)→193(L) (89%)	189→194 (7%)		8.25	0.0	1.0	0.1	747	0.75
1.67	741	0.91	192→194 (89%)	189→193 (7%)		6.89	1.0	0.0	0.0	727	0.77
2.07	598	0.00	192→195 (99%)			11.2	0.0	1.0	0.0	592	0.00
2.71	458	0.01	192→196 (88%)	192→198 (10%)		7.84	0.0	0.1	1.0	453	0.00
2.75	451	0.04	192→196 (12%)	192→198 (81%)	192→199 (3%)	3.24	0.0	0.1	1.0	439	0.03
$ZnPcPh_8$, **6**											
1.57	788	0.76	220(H)→221(L) (89%)	219→222 (6%)	216→222 (2%)	9.48	0.0	1.0	0.0	783	0.65
1.59	781	0.84	220→222 (89%)	219→221 (6%)	216→221 (2%)	6.46	1.0	0.0	0.0	768	0.71
1.95	637	0.00	220→223 (99%)			10.8	0.0	1.0	0.0	622	0.00
2.55	487	0.17	220→224 (68%)	220→225 (29%)		3.65	0.1	0.0	1.0	473	0.05
2.60	477	0.04	220→224 (31%)	220→225 (68%)		7.12	0.2	0.0	1.0	464	0.09

umns of Table 4, from left to right. In addition, transition wavelengths and oscillator strengths of the phenyl-removed Pcs (these are represented as **2***, **3***, and so forth) are also provided in the two right-hand columns of Table 4; the structures of the phenyl-removed Pcs were modeled by replacing the phenyl groups of the optimized structures with hydrogen atoms, the latter being placed in the standard positions as aromatic protons. MO calculations of unsubstituted Zn^{II} Pc have been reported previously in the literature,[46,47] and our results are basically similar to these, with an intense Q-band predicted in the visible region (ca. 720 nm), composed mainly of HOMO→LUMO transitions (ca. 90%). The lowest-energy bands (the Q-bands) of **6** are calculated to lie at 788 and 781 nm, while the experimentally observed wavelength is 786 nm. The Q-band energy increases with decreasing number of phenyl groups: 747 and 741 nm and 733 and 728 nm for **5** and **4**, respectively. These are also in close agreement with the experimental values (732 and 704 nm for **5** and **4**, respectively). Similarly to **1**, the HOMO→LUMO transitions account for about 90% of the Q-band excited state in the CI calculations for **2**–**6**, which indicates that the ring deformations do not significantly change the composition of the Q-band. Figure 11 shows the frontier MO energy diagram of **1**–**6**. Since both the LUMO and

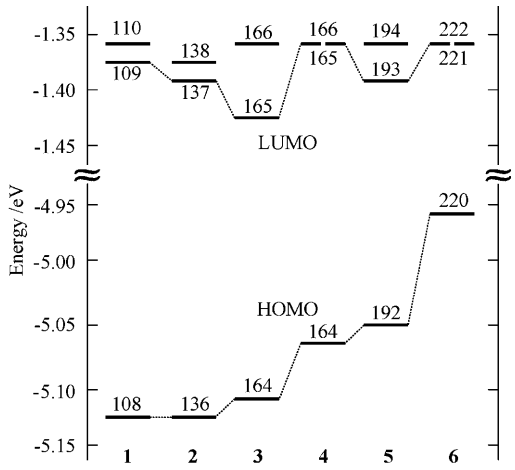

Figure 11. Frontier MO energy diagram for **1**–**6**.

LUMO+1 orbitals contribute significantly to the Q-bands, the average energy of the LUMO and LUMO+1 levels should be regarded as the LUMO energy during analysis of the impact of trends in the HOMO-LUMO gaps on the absorption spectra. The energy gap between the HOMO and "midpoint" LUMO levels is 3.77, 3.75, 3.72, 3.71, 3.67, and 3.60 eV for **1**–**6**, respectively. The same trend is observed in the Q-band energies as phenylation increases on going from **1** to **6**. It should be noted that the LUMO and LUMO+1 energies split even in the case of **1** because of the presence of the axial pyridine ligand. The largest splitting was calculated for **3** and the second largest for **5**, reflecting the lower symmetry of the phenyl substitutions in these complexes. Unlike the LUMO energy, the LUMO+1 energies do not shift markedly from complex to complex.

The Q-band of **6*** was calculated to lie at 783 nm, which is close to the wavelength calculated for **6** (788 nm), suggesting that the presence of the phenyl groups has only a limited effect on the Q-band energy. Similar results were obtained for **2**–**5**, with the lowest energy bands appearing almost at identical positions for the phenyl-substituted and unsubstituted derivatives. For example, the lowest-energy bands for **2**–**5** were calculated to lie at 729, 736, 733, and 747 nm, respectively, and those for **2***–**5*** at 723, 723, 730, and 747 nm, respectively. This result can be understood by considering the distribution of the nodal patterns of the HOMO, LUMO, and LUMO+1. As depicted in Figure 12, the nodes of these three MOs are localized on the Pc ligand rather than the phenyl groups. Therefore, the destabilization of the HOMOs originates not from the phenyl substitution, but from ring deformation. The MO calculations can also be used to assign the moderately intense band observed at around 429 nm in the absorption spectrum of **6**. This band is also observed for **5**, together with an accompanying MCD *B*-term (Figure 7). INDO/S calculations predict that these transitions originate mainly from the HOMO→LUMO+3 transition (68%), with an oscillator strength of 0.17 in the case of **6**. The molecular symmetries of the π systems of **1** and **6** can be assumed to be D_{4h} and D_{2d}, respectively. The HOMO→LUMO+3 transition of **6** is therefore symmetry-allowed, while the corresponding transition for **1** is parity-forbidden with a calculated oscillator strength of 0.00. Since this transition contains 29% of the HOMO→LUMO+4 transition and MO coefficients of LUMO+4 are spread over the entire complex, including the phenyl groups, the presence of the phenyl groups plays an important role in increasing the band intensity in this region of the spectrum. In the calculation for **6***, the calculated oscillator strength of the 429 nm band is roughly halved. The presence of this band provides another piece of evidence that the structure of **6** is highly deformed even in solution. Although we have reported these kinds of ligand deformation-induced transitions previously for an octaphenylated FePc in which parity-forbidden MLCTs become allowed due to ring deformations,[10] this is the first example of a π–π* band of a Pc π system induced by saddle-type deformation. Gouterman has previously reported that shuttlecock-shaped PbPc (C_{4v} symmetry) displays a *z*-polarized transition due to the non-planarity of the ligand.

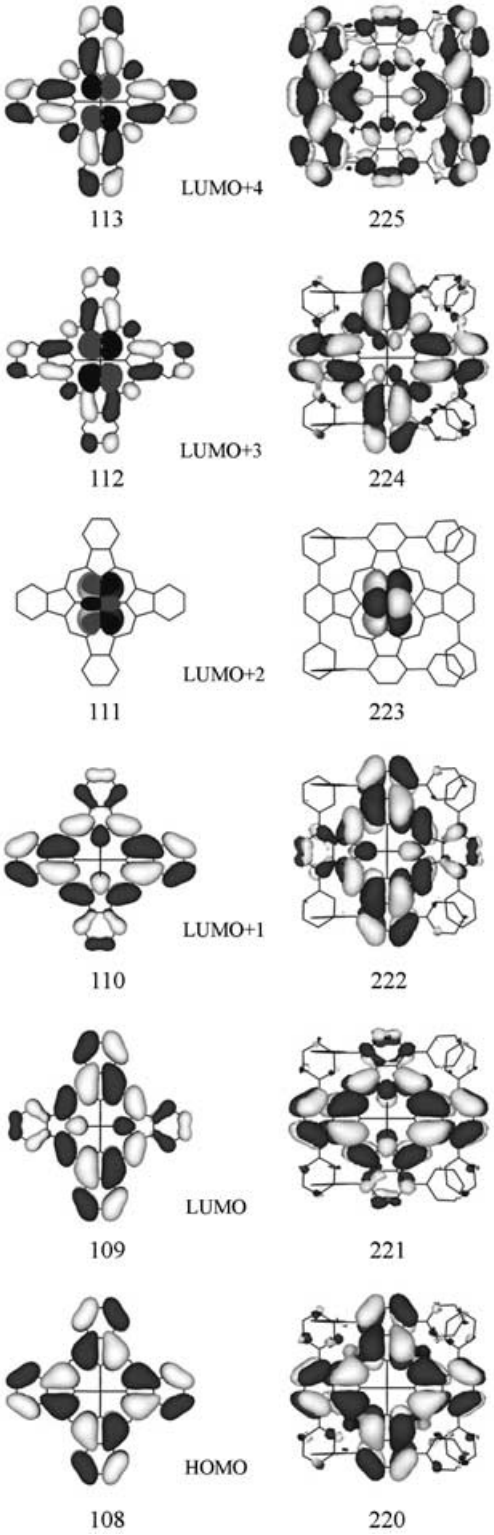

Figure 12. Selected views of MOs of **1** (left) and **6** (right). The LUMO+2s (111 and 223 for **1** and **6**, respectively) are pyridine-centered orbitals. See Supporting Information for the MOs of the other derivatives.

Conclusion

A series of Zn^{II} Pcs bearing phenyl substituents at the 1-, 4-, 8-, 11-, 15-, 18-, 22-, and/or 25-positions has been synthesized and characterized by various spectroscopic and electrochemical methods, including ^1H NMR, MALDI-TOF mass spectrometry, X-ray crystallography, absorption and MCD spectroscopy, and electrochemical measurements. Using 3,6-diphenylphthalonitrile and *o*-phthalonitrile as starting materials, a metal template reaction and the lithium method resulted in markedly different product ratios. The template reaction using Zn^{II} ions gave predominantly near-planar derivatives (**1**–**3**), while the lithium method resulted in substantially higher yields of sterically hindered derivatives. The ^1H NMR spectra of the new compounds are fully consistent with the expected molecular structures, and the opposite and adjacent isomers (**3** and **4**) could be unambiguously assigned. The X-ray crystal structures of **5** and **6** revealed highly deformed ligands, while the molecules in the crystals of **2** are planar. Interestingly, the crystal structure of **4** was found to be relatively planar, although the overlap of the substituted phenyl groups may contribute to the ring deformation. Inspection of the crystal packing arrangements revealed that the strong π–π stacking force pushes the ring deformations back to planar conformations. DFT geometry optimization calculations predict that **4**–**6** will have deformed conformations in solution, however. The Q-band shifts to the red with increasing number of phenyl groups, and a negative shift of the first oxidation potential is observed. These physicochemical data have been considered in combination with the results of MO calculations. The trends in the redox potentials from complex to complex correlate reasonably well with the results of the calculated MO energies. Configuration interaction calculations based on the INDO/S Hamiltonian reproduced the major experimentally observed spectral features. Calculations for **2***–**6*** (**2**–**6** with the phenyl groups removed and replaced with hydrogen atoms) also showed similar Q-band energies. The present study has therefore revealed that sizable red shifts of the Q-band in highly deformed Pcs are brought about mainly by the ring deformations. In addition, the reduced symmetry results in the HOMO→LUMO+3 transition, which is parity-forbidden in the case of **1**, gaining significant intensity at about 430 nm in the absorption spectrum of **6**.

Experimental Section

Measurements: ^1H NMR spectra were recorded using a JEOL GSX-400 (400 MHz) spectrometer. MALDI mass spectra were measured on a Voyager STR spectrometer using dithranol as the matrix. Crystal structure analyses were performed on a Rigaku/MSC Mercury diffractometer using graphite-monochromated $Mo_{K\alpha}$ radiation. The structures were solved by heavy-atom Patterson methods and expanded using Fourier techniques. Hydrogen atoms were refined isotropically, while those of other elements were refined anisotropically. The crystal data and experimental details are summarized in Table 1.

Electronic absorption spectra were measured with a Hitachi U-3410 spectrophotometer. Magnetic circular dichroism (MCD) spectra were recorded using a Jasco J-725 spectrodichrometer with a Jasco electromagnet that produces a magnetic field of up to 1.09 T. The magnitude of the MCD signal is expressed in terms of molar ellipticity per tesla, $[\theta]_M$/deg·mol^{-1} dm^3 cm^{-1} T^{-1}.

Cyclic voltammetry data were collected with a Hokuto Denko HA-501 potentiostat connected to a Hokuto Denko HB-104 function generator and a Graphtec WX1200 XY recorder. *o*-Dichlorobenzene (*o*-DCB, HPLC grade) was used as the solvent with 0.1 mol L^{-1} tetrabutylammonium perchlorate (TBAP) as the supporting electrolyte. Glassy carbon (area = 0.07 cm^2), Pt, and Ag/AgCl wires were used as working, counter, and reference electrodes, respectively. The ferrocenium/ferrocene (Fc^+/Fc) couple (observed at 415 ± 15 mV versus Ag/AgCl) was used as an internal standard.

Molecular orbital calculations: DFT geometry optimizations were carried out using the B3LYP hybrid functional and the 6–31G(d) basis set. The initial geometries were taken from the crystal structure if available. Both the HyperChem[48] and Reimer[49] software packages were used for configuration interaction (CI) calculations using the INDO/S Hamiltonian. The lowest 20 one-electron excitations were included in the CI calculations. In the case of hypothetically phenyl-removed Pcs (see the MO calculation section for details), phenyl groups were simply removed from the optimized structure and protons added with the normal bond lengths and angles.

Synthesis: Unsubstituted ZnPc (**1**)[50] and 3,6-diphenylphthalonitrile[51] were prepared according to the literature. The α-phenyl-substituted Pcs, with the exception of $ZnPcPh_8$ (**6**), were obtained by way of a mixed condensation reaction between phthalonitrile and 3,6-diphenylphthalonitrile. The yields of each complex were calculated on the basis of the total nitrile starting material. Although **6** could be obtained as a minor product of the mixed condensation, it was synthesized separately in order to avoid the difficult purification procedures. All chemicals were used as supplied.

[1,4-Diphenylphthalocyaninato]zinc(II) ($ZnPcPh_2$, 2), [1,4,15,18-tetraphenylphthalocyaninato]zinc(II) (*opp*-$ZnPcPh_4$, 3), [1,4,8,11-tetraphenylphthalocyaninato]zinc(II) (*adj*-$ZnPcPh_4$, 4), and [1,4,8,11,15,18-hexaphenylphthalocyaninato]zinc(II) ($ZnPcPh_6$, 5)

Method 1 (lithium method): Lithium (25 mg) was added to 1-hexanol (3 mL), and the solution was stirred at 170 °C for 1 h. After the mixture had been cooled to room temperature, a mixture of *o*-phthalonitrile (600 mg, 2.14 mmol) and 3,6-diphenylphthalonitrile (140 mg, 1.09 mmol) was added. The solution was then heated at 170 °C for 1 h. The resultant dark colored product was purified by column chromatography on silica (toluene as eluent) to give three types of metal-free phenyl-substituted Pc derivative. Unsubstituted H_2Pc, formed during the course of the reaction, was strongly adsorbed onto the core of the column, and was therefore removed completely from the eluate. Each metal-free derivative was dissolved in DMF (ca. 3 mL), and zinc acetate (200 mg) was added. The respective mixtures were refluxed at 170 °C for 45 min. The colored products were purified by column chromatography on alumina (toluene/pyridine = 25:1 (v/v) as eluent), and recrystallized from toluene/methanol to give **2**, **4**, and **5** in yields of 16.5, 2.7, and 7.1 %, respectively.

Method 2 (template reaction): A mixture of *o*-phthalonitrile (600 mg, 2.14 mmol), 3,6-diphenylphthalonitrile (140 mg, 1.09 mmol), zinc acetate (200 mg), and a catalytic amount of hydroquinone was placed in a screw-capped test tube under a nitrogen atmosphere. The reaction was conducted at 270 °C for 20 min using a bath of molten tin. Column chromatography on alumina (toluene/pyridine, 25:1 (v/v) as eluent), followed by recrystallization from toluene/methanol, gave **2** and **3** in yields of 10.5 and 3.4 %, respectively.

MALDI-MS (*m*/*z*): 729 ([M^++1] for **2**), 881 ([M^++1] for **3**), 880 ([M^+] for **4**), 1033 ([M^++1] for **5**); elemental analysis calcd (%) for $C_{44}H_{24}N_8Zn$ (**2**): C 72.38, H 3.31, N 15.35; found: C 72.00, H 3.59, N 15.21; elemental analysis calcd (%) for $C_{56}H_{32}N_8Zn$ (**3**): C 76.23, H 3.66, N 12.70; found: C 76.41, H 4.17, N 12.36; elemental analysis calcd (%) for $C_{56}H_{32}N_8Zn$ (**4**): C 76.23, H 3.66, N 12.70; found: C 75.55, H 3.92, N 12.48; elemental analysis calcd (%) for $C_{68}H_{40}N_8Zn$ (**5**): C 78.95, H 3.90, N 10.83; found:

C 78.76, H 4.32, N 10.97; ^{1}H NMR ([D$_5$]pyridine, 400 MHz): for **2**, δ = 9.70 (m, 4H), 9.04 (m, 2H), 8.55 (dd, 4H), 8.19 (m, 8H), 7.96 ppm (m, 6H); for **3**, δ = 9.03 (dd, 4H), 8.50 (q, 8H), 8.13 (m, 8H), 7.93 ppm (m, 12H); for **4**, δ = 9.65 (d, 2H), 8.92 (d, 2H), 8.41 (d, 4H), 8.38–7.83 (m, 18H), 7.47–7.35 ppm (m, 6H); for **5**, δ = 8.87 (dd, 2H), 8.40 (dd, 4H), 8.05–7.71 (m, 20H), 7.45–7.32 ppm (m, 12H).

[1,4,8,11,15,18,22,25-Octaphenylphthalocyaninato]zinc(II) (ZnPcPh$_8$, 6): This compound was derived from metal-free H_2PcPh_8[8] by way of a metal-insertion reaction as described above. MALDI-MS (*m*/*z*): 1185 ([M^++1]); elemental analysis calcd. for $C_{80}H_{48}N_8Zn$ (**6**): C 80.97, H 4.08, N 9.44; found: C 81.02, H 4.53, N 9.58; ^{1}H NMR ([D$_5$]pyridine, 400 MHz): δ = 7.72–7.66 (m, 16H), 7.56 (8H, this signal overlaps with a solvent signal), 7.44–7.31 ppm (m, 24H).

Acknowledgements

This research was supported by a Grant-in-Aid for the COE project, Giant Molecules and Complex Systems, 2005, and Grant for Encouragement of Young Scientists (B) No. 17750029 and that for Scientific Research (B) No. 17350063 from the Ministry of Education, Culture, Sports, Science, and Technology, Japan. Some of the results of this research were obtained using the supercomputing resources at the Information Synergy Center, Tohoku University.

[1] A. Braun, J. Tcherniac, *Chem. Ber.* **1907**, *40*, 2709.
[2] a) J. M. Robertson, *J. Chem. Soc.* **1935**, 615; b) J. M. Robertson, *J. Chem. Soc.* **1936**, 1195.
[3] a) *The Porphyrin Handbook*, *Vols. 15–20* (Eds.: K. M. Kadish, K. M. Smith, R. Guilard), Academic Press, San Diego, **2003**; b) *Phthalocyanine Materials – Synthesis, Structure and Function* (Ed.: N. B. McKeown), Cambridge University Press, Cambridge, **1998**; c) *Phthalocyanines – Properties and Applications*, *Vols. I–IV* (Eds.: C. C. Leznoff, A. B. P. Lever), VCH, New York, **1989**, **1992**, **1993**, **1996**; d) *The Phthalocyanines*, *Vols. 1–2* (Eds.: F. H. Moser, A. H. Thomas), CRC Press, Boca Raton, FL, **1983**.
[4] There are 16 carbon atoms on the Pc periphery, of which the eight equivalent positions closer to (i. e., the 1-, 4-, 8-, 11-, 15-, 18-, 22-, and 25-positions) and eight equivalent positions furthest away (i. e., the 2-, 3-, 9-, 10-, 16-, 17-, 23-, and 24-positions) from the inner Pc perimeter are often termed as the α- and β-positions, respectively (N. Kobayashi, N. Sasaki, Y. Higashi, T. Osa, *Inorg. Chem.* **1995**, *34*, 1636). The usage of α and β in this paper is therefore not related to the nomenclature used for the polymorphs of Pcs. α-Phenyl-substituted Pc, for example, denotes Pcs substituted by phenyl groups at the α-positions.
[5] M. K. Engel in *The Porphyrin Handbook*, *Vol. 20* (Eds.: K. M. Kadish, K. M. Smith, R. Guilard), Academic Press, San Diego, **2003**, Chapter 122.
[6] a) Y. Iyechika, K. Yakushi, I. Ikemoto, H. Kuroda, *Acta Crystallogr. Sect. B* **1982**, *38*, 766; b) K. Ukei, *Acta Crystallogr. Sect. B* **1973**, *29*, 2290.
[7] L. Chambrier, M. J. Cook, P. T. Wood, *Chem. Commun.* **2000**, 2133.
[8] N. Kobayashi, T. Fukuda, K. Ueno, H. Ogino, *J. Am. Chem. Soc.* **2001**, *123*, 10740.
[9] H. Lee, W. W. Brennessel, J. A. Lessing, W. W. Brucker, V. G. Young Jr., S. M. Gorun, *Chem. Commun.* **2003**, 1576.
[10] T. Fukuda, S. Homma, N. Kobayashi, *Chem. Commun.* **2003**, 1574.
[11] T. Fukuda, K. Ono, S. Homma, N. Kobayashi, *Chem. Lett.* **2003**, *32*, 736.
[12] a) G. J. Bodwell, J. N. Bridson, M. K. Cyrañski, J. W. J. Kennedy, T. M. Krygowski, M. R. Mannion, D. O. Miller, *J. Org. Chem.* **2003**, *68*, 2089; b) G. J. Bodwell, D. O. Miller, R. J. Vermeij, *Org. Lett.* **2001**, *3*, 2093; c) G. J. Bodwell, J. J. Fleming, D. O. Miller, *Tetrahedron* **2001**, *57*, 3577; d) G. J. Bodwell, J. J. Fleming, M. R. Mannion, D. O. Miller, *J. Org. Chem.* **2000**, *65*, 5360; e) G. J. Bodwell, J. N. Bridson, T. J. Houghton, J. W. J. Kennedy, M. R. Mannion, *Chem. Eur. J.* **1999**, *5*, 1823; f) G. J. Bodwell, J. N. Bridson, T. J. Houghton, J. W. J. Kennedy, M. R. Mannion, *Angew. Chem.* **1996**, *108*, 1418; *Angew. Chem. Int. Ed. Engl.* **1996**, *35*, 1320.
[13] M. Bühl, A. Hirsch, *Chem. Rev.* **2001**, *101*, 1153, and references therein.
[14] a) M. O. Senge in *The Porphyrin Handbook*, *Vol. 1* (Eds.: K. M. Kadish, K. M. Smith, R. Guilard), Academic Press, San Diego, **2000**, Chapter 6, and references therein; b) H. S. Gill, M. Harmjanz, J. Santamaría, J. I. Finger, M. J. Scott, *Angew. Chem.* **2004**, *116*, 491; *Angew. Chem. Int. Ed.* **2004**, *43*, 485; c) T. Picaud, C. L. Moigne, B. Loock, M. Momenteau, A. Desbois, *J. Am. Chem. Soc.* **2003**, *125*, 11616; d) J. L. Retsek, C. M. Drain, C. Kirmaier, D. J. Nurco, C. J. Medforth, K. M. Smith, I. V. Sazanovich, V. S. Chirvony, J. Fajer, D. Holten, *J. Am. Chem. Soc.* **2003**, *125*, 9787; e) I. H. Wasbotten, J. Conradie, A. Ghosh, *J. Phys. Chem. B* **2003**, *107*, 3613; f) R. E. Haddad, S. Gazeau, J. Pecaut, J. Marchon, C. J. Medforth, J. A. Shelnutt, *J. Am. Chem. Soc.* **2003**, *125*, 1253; g) T. Ikeue, Y. Ohgo, M. Nakamura, *Chem. Commun.* **2003**, 220; h) H. Ryeng, A. Ghosh, *J. Am. Chem. Soc.* **2002**, *124*, 8099.
[15] a) C. G. Claessens, D. González-Rodríguez, T. Torres, *Chem. Rev.* **2002**, *102*, 835; b) C. G. Claessens, D. González-Rodríguez, B. del Rey, T. Torres, G. Mark, H. Schuchmann, C. von Sonntag, J. G. MacDonald, R. S. Nohr, *Eur. J. Org. Chem.* **2003**, 2547; c) T. Fukuda, M. M. Olmstead, W. S. Durfee, N. Kobayashi, *Chem. Commun.* **2003**, 1256; d) C. G. Claessens, T. Torres, *J. Am. Chem. Soc.* **2002**, *124*, 14522; e) C. G. Claessens, T. Torres, *Angew. Chem.* **2002**, *114*, 2673; *Angew. Chem. Int. Ed.* **2002**, *41*, 2561; f) T. Fukuda, J. R. Stork, R. J. Potucek, M. M. Olmstead, B. C. Noll, N. Kobayashi, W. S. Durfee, *Angew. Chem.* **2002**, *114*, 2677; *Angew. Chem. Int. Ed.* **2002**, *41*, 2565.
[16] N. B. McKeown in *The Porphyrin Handbook*, *Vol. 15* (Eds.: K. M. Kadish, K. M. Smith, R. Guilard), Academic Press, San Diego, **2003**, Chapter 98, and references therein.
[17] E. A. Ohgh, M. J. Stillman, *Inorg. Chem.* **1994**, *33*, 573.
[18] a) J. Mack, M. J. Stillman, *Inorg. Chem.* **2001**, *40*, 812; b) J. Mack, M. J. Stillman, *J. Phys. Chem.* **1995**, *99*, 7935.
[19] T. Fukuda, N. Kobayashi, *Chem. Lett.* **2002**, 866.
[20] N. Kobayashi, T. Fukuda, *J. Am. Chem. Soc.* **2002**, *124*, 8021.
[21] a) K. J. M. Nolan, M. J. Hu, C. C. Leznoff, *Synlett* **1997**, 593; b) S. W. Oliver, T. D. Smith, *J. Chem. Soc. Perkin Trans. 2* **1987**, 1579.
[22] N. Kobayashi, H. Miwa, V. N. Nemykin, *J. Am. Chem. Soc.* **2002**, *124*, 8007.
[23] N. Kobayashi, T. Ashida, T. Osa, H. Konami, *Inorg. Chem.* **1994**, *33*, 1735.
[24] T. J. Hurley, M. A. Robinson, S. I. Trotz, *Inorg. Chem.* **1967**, *6*, 389.
[25] T. Fukuda, N. Kobayashi, *J. Porphyrins Phthalocyanines* **2004**, *8*, 1251.
[26] a) H. Hückstädt, C. Jaouen, M. Göldner, U. Cornelissen, A. Tutaß, A. H. Homborg, *Z. Anorg. Allg. Chem.* **2000**, *626*, 671; b) M. Mossoyan-Deneux, D. Benlian, M. Pierrot, A. Fournel, J.-P. Sorbier, *Inorg. Chem.* **1985**, *24*, 1878; c) M. Mossoyan-Deneux, D. Benlian, M. Ley, M. Pierrot, J. P. Sorbier, A. Fournel, *Mol. Cryst. Liq. Cryst.* **1985**, *120*, 437; d) T. Kobayashi, T. Ashida, N. Uyeda, E. Suito, M. Kakudo, *Bull. Chem. Soc. Jpn.* **1971**, *44*, 2095.
[27] B. A. Bench, A. Beveridge, W. M. Sharman, G. J. Diebold, J. E. van Lier, S. M. Gorun, *Angew. Chem.* **2002**, *114*, 773; *Angew. Chem. Int. Ed.* **2002**, *41*, 748.
[28] W. R. Scheidt, Y.-J. Lee, *Struct. Bonding (Berlin)* **1987**, *64*, 1.
[29] To verify the energy required to modify the ligand structure in the crystalline state, single-point total energies for both the crystal and DFT-optimized structures were calculated at the INDO/S level. The energy differences are 0.42, 0.51, 0.73, and 0.78 a. u. for **2**, **4**, **5**, and **6**, respectively. These values are within the calculation errors for both the planar and deformed derivatives. Therefore, the calculations predict that the structural stresses seen in these crystals do not require a large packing energy.
[30] In relation to this, it is known that biphenyl is most stable when the torsion angle is about 45°: a) A. Almenningen, O. Bastiansen, L. Fernholt, B. N. Cyvin, S. J. Cyvin, S. Samdal, *J. Mol. Struct.* **1985**,

128, 59; b) A. Hargreaves, S. H. Rizvi, *Acta Crystallogr.* **1962**, *18*, 365; c) F. Grein, *J. Mol. Struct.* **2003**, *624*, 23, and references therein).

[31] a) T. Sugimori, M. Torikata, J. Nojima, S. Tominaka, K. Tobikawa, M. Handa, K. Kasuga, *Inorg. Chem. Commun.* **2002**, *5*, 1031; b) T. Sugimori, S. Okamoto, N. Kotoh, M. Handa, K. Kasuga, *Chem. Lett.* **2000**, 1200; c) S. A. Mikhalenko, S. A. Gladyr′, E. A. Luk′yanets, *Zh. Org. Khim.* **1972**, *8*, 341; d) S. A. Mikhalenko, E. A. Luk′yanets, *Zh. Obshch. Khim.* **1969**, *39*, 2129.

[32] H. Konami, H. Hatano, *Chem. Lett.* **1988**, 1359.

[33] To confirm the "additivity", we have synthesized a series of *para*-substituted α-octaphenyl Pcs, that is, αααα, αααβ, αβαβ(opp), ααββ-(adj), and ββββ, where α denotes 3,6-diphenylphthalonitrile units and β denotes 3,6-bis(4-methoxyphenyl)-4,5-dicyanobenzene units. The ligand deformations are expected to be almost identical from complex to complex on the basis of the molecular structures, and they show reasonable additivities of the Q-band energies with respect to the number of methoxy groups. In particular, the opposite and adjacent isomers show practically identical Q-band energies (i. e., 800 and 801 nm for metal-free αβαβ and ααββ isomers, respectively). T. Fukuda, *Doctoral Thesis*, Tohoku University, **2004**.

[34] a) A. K. Wertsching, A. S. Koch, S. G. DiMagno, *J. Am. Chem. Soc.* **2001**, *123*, 3932; b) S. G. DiMagno, A. K. Wertsching, C. R. Ross, *J. Am. Chem. Soc.* **1995**, *117*, 8279.

[35] H. Ryeng, A. Ghosh, *J. Am. Chem. Soc.* **2002**, *124*, 8099.

[36] R. E. Haddad, S. Gazeau, J. Pécaut, J. Marchon, C. J. Medforth, J. A. Shelnutt, *J. Am. Chem. Soc.* **2003**, *125*, 1253.

[37] L. Edwards, M. Gouterman, *J. Mol. Spectr.* **1970**, *33*, 292.

[38] T. Fukuda, E. A. Makarova, E. A. Luk′yanets, N. Kobayashi, *Chem. Eur. J.* **2004**, *10*, 117.

[39] Electrochemical data for several unsubstituted or *t*-butylated ZnPcs are available in the literature (ref. [40]).

[40] a) M. L′her, A. Pondaven in *The Porphyrin Handbook*, *Vol. 16* (Eds.: K. M. Kadish, K. M. Smith, R. Guilard), Academic Press, San Diego, **2003**, Chapter 104; b) A. Wolberg, J. Manassen, *J. Am. Chem. Soc.* **1970**, *92*, 2982; c) D. Lexa, M. Reix, *J. Chem. Phys.* **1974**, *71*, 511; d) D. W. Clack, N. S. Hush, I. S. Woolsey, *Inorg. Chim. Acta* **1976**, *19*, 129; e) A. Giraudeau, F. F. Fau, A. J. Bard, *J. Am. Chem. Soc.* **1980**, *102*, 5137; f) H. Homborg, K. S. Murray, *Z. Anorg. Allg. Chem.* **1984**, *517*, 149; g) B. Schöllhorn, J. P. Germain, A. Pauly, C. Maleysson, J. P. Blanc, *Thin Solid Films* **1998**, *326*, 245; h) K. Hesse, D. Schlettwein, *J. Electroanal. Chem.* **1999**, *476*, 148; i) S. V. Vulf'son, O. L. Kaliya, O. L. Lebedev, E. A. Luk′yanets, *Zh. Org. Khim.* **1976**, *12*, 123; j) V. I. Gavrilov, L. G. Tomilova, I. V. Shelepin, E. A. Luk′yanets, *Elektrokhimiya* **1979**, *15*, 1058; k) V. I. Gavrilov, E. A. Luk′yanets, I. V. Shelepin, *Elektrokhimiya* **1981**, *17*, 1183; l) A. B. P. Lever, S. Licoccia, B. S. Ramaswamy, S. A. Kandil, D. V. Stynes, *Inorg. Chim. Acta* **1981**, *51*, 169; m) R. H. Campbell, G. A. Heath, G. I. Hefter, R. C. S. McQueen, *J. Chem. Soc. Chem. Commun.* **1983**, 1123; n) E. P. Platonova, E. Y. Skuridin, L. S. Degtyarev, *Zh. Obshch. Khim.* **1984**, *54*, 925; o) A. Gouloumis, S.-G. Liu, A. Sastre, P. Vazquez, L. Echegoyen, T. Torres, *Chem. Eur. J.* **2000**, *6*, 3600.

[41] a) J. H. Fuhrhop, P. Wasser, D. Riesner, D. Mauzeral, *J. Am. Chem. Soc.* **1972**, *94*, 7996; b) H. Song, C. A. Reed, W. R. Scheidt, *J. Am. Chem. Soc.* **1989**, *111*, 6865; c) C. Z. Schulz, H. Song, A. Mislanker, R. D. Orosz, C. A. Reed, P. G. Debrunner, W. R. Scheidt, *Inorg. Chem.* **1997**, *36*, 406.

[42] a) J. Mack, M. J. Stillman, *Inorg. Chem.* **1997**, *36*, 413; b) J. Mack, M. J. Stillman, *J. Am. Chem. Soc.* **1994**, *116*, 1292; c) T. Nyokong, Z. Gasyna, M. J. Stillman, *Inorg. Chem.* **1987**, *26*, 1087.

[43] A. B. P. Lever, E. R. Milaeva, G. Speier, in *Phthalocyanines – Properties and Applications*, *Vol. III* (Eds.: C. C. Leznoff, A. B. P. Lever), VCH, New York, **1993**, Chapter 1.

[44] N. Kobayashi, H. Konami, in *Phthalocyanines – Properties and Applications*, *Vol. IV* (Eds.: C. C. Leznoff, A. B. P. Lever), VCH, New York, **1996**, Chapter 9.

[45] M. J. Frisch, G. W. Trucks, H. B. Schlegel, G. E. Scuseria, M. A. Robb, J. R. Cheeseman, V. G. Zakrzewski, J. A. Montgomery Jr., R. E. Stratmann, J. C. Burant, S. Dapprich, J. M. Millam, A. D. Daniels, K. N. Kudin, M. C. Strain, O. Farkas, J. Tomasi, V. Barone, M. Cossi, R. Cammi, B. Mennucci, C. Pomelli, C. Adamo, S. Clifford, J. Ochterski, G. A. Petersson, P. Y. Ayala, Q. Cui, K. Morokuma, N. Rega, P. Salvador, D. D. Dannenberg, D. K. Malick, A. D. Rabuck, K. Raghavachari, J. B. Foresman, J. Cioslowski, J. V. Ortiz, A. G. Baboul, B. B. Stefanov, G. Liu, A. Liashenko, P. Piskorz, I. Komaromi, R. Gomperts, R. L. Martin, D. J. Fox, T. Keith, M. A. Al-Laham, C. Y. Peng, A. Nanayakkara, M. Challacombe, P. M. W. Gill, B. Johnson, W. Chen, M. W. Wong, J. L. Andres, C. Gonzalez, M. Head-Gordon, E. S. Replogle, J. A. Pople, *Gaussian 98*, *Revision A.11.3*, Gaussian, Inc., Pittsburgh, PA, **2002**.

[46] G. Ricciardi, A. Rosa, E. J. Baerends, *J. Phys. Chem. A* **2001**, *105*, 5242.

[47] E. J. Baerends, G. Ricciardi, A. Rosa, S. J. van Gisbergen, *Coord. Chem. Rev.* **2002**, *230*, 5.

[48] HyperChem Pro software package, Hypercube, Inc., Gainesville, FL, USA, **1997**.

[49] J. R. Reimer, School of Chemistry, University of Sydney, NSW, Australia, **1997**.

[50] P. A. Barret, C. E. Dent, R. P. Linstead, *J. Chem. Soc.* **1936**, 1719.

[51] S. A. Mikhalenko, S. A. Glandyr, E. A. Luk′yanets, *Russ. J. Org. Chem.* **1972**, *8*, 341.

Received: February 18, 2005
Published online: June 23, 2005